Journal of Materials Chemistry C

RSC Publishing

PAPER

View Article Online
View Journal | View Issue

Cite this: J. Mater. Chem. C, 2013, 1, 1970

Synthesis of bulk-size transparent gadolinium oxide–polymer nanocomposites for gamma ray spectroscopy

Wen Cai,†[ad] Qi Chen,†[a] Nerine Cherepy,[b] Alex Dooraghi,[c] David Kishpaugh,[a] Arion Chatziioannou,[c] Stephen Payne,[b] Weidong Xiang[d] and Qibing Pei*[a]

Received 20th September 2012
Accepted 22nd December 2012

DOI: 10.1039/c2tc00245k

www.rsc.org/MaterialsC

Heavy element loaded polymer composites have long been proposed to detect high energy X- and γ-rays upon scintillation. The previously reported bulk composite scintillators have achieved limited success because of the diminished light output resulting from fluorescence quenching and opacity. We demonstrate the synthesis of a transparent nanocomposite comprising gadolinium oxide nanocrystals uniformly dispersed in bulk-size samples at a high loading content. The strategy to avoid luminescence quenching and opacity in the nanocomposite was successfully deployed, which led to the radioluminescence light yield of up to 27 000/MeV, about twice as much as standard commercial plastic scintillators. Nanocomposites monoliths (14 mm diameter by 3 mm thickness) with 31 wt% loading of nanocrystals generated a photoelectric peak for Cs-137 gamma (662 keV) with 11.4% energy resolution.

Introduction

Nanocomposites comprising a high loading content of nanoparticles dispersed in a polymer matrix are being extensively investigated for various electronic, photonic, and mechanical applications.[1,2] They have recently been proposed to detect high energy X- and γ-rays, with the potential to be deployed in fields such as medical imaging, cosmic study, nuclear industry and biological research.[3,4] In the proposed nanocomposites, the polymer matrix provides short scintillation time with a low fabrication cost. The embedded nanoparticles not only increase the nanocomposite density for enhanced stopping power of high energy photons, but also increase the effective atomic numbers (Z_{eff}) leading to a higher photoelectric effect ratio. Therefore, the nanocomposites are expected to provide energy resolution of the photoelectric peak when detecting high energy X- and γ-rays.

Since the middle of the last century, composites loaded with organometallics as gamma sensitizers to increase Z_{eff} and density have been widely reported.[5–12] However, even a small loading of organometallics led to luminescence quenching and resulted in critical reduction of light yield in composite scintillators. While the quenching mechanisms have not been completely resolved,[13–15] the working mechanisms have been proposed as the following: the polymer matrix and the dissolved organometallics have comparable energy band gaps. Excitons (excited states) generated on the polymer can transfer their energy to either the organometallics or the fluors. The fluors receive a portion of energy from the matrix and decay radiatively to produce visible photons readily detectable by a photomultiplier tube (PMT). However, the excited organometallics barely contribute to the final light yield. This is because they usually decay non-radiatively, and their possible interaction with the excitons *via* spin–orbit coupling may produce predominately triplet excitons, whose energy cannot be transferred to standard organic fluors due to the selection rule. Therefore, the portion of energy involving excited organometallics is wasted *via* vibrational thermalization, which is responsible for the poor light yield.

To achieve a high light yield, new approaches to high-*Z* composite materials have been suggested. Conjugated polymer (CP) composites containing inorganic high-*Z* compounds have been proposed to serve as an alternative to the conventional matrix.[16,17] Employing high-*Z* ingredients with a band gap larger than that of the CP matrix has been demonstrated to facilitate energy transfer in the composite to generate visible photons efficiently. Later on, composites comprised of triphenylbismuth, polyvinylcarbazole, and a triplet emitter were reported by Rupert *et al.*, which exhibited an improved light yield and produced a gamma photoelectric peak.[18] However, most high-*Z* organometallics including triphenylbismuth are thermally unstable due to the low enthalpy of the metal–carbon bond (*ca.* 2 eV for the Bi–C bond in triphenylbismuth).[19] Organometallics are also known to undergo photolytic bond homolysis to introduce impurities that could quench the luminescence.[20]

[a]Department of Materials Science and Engineering, University of California, Los Angeles, CA 90095-1595, USA. E-mail: qpei@seas.ucla.edu; Tel: +1 310 825 4127

[b]Lawrence Livermore National Laboratory, Livermore, CA 94550, USA

[c]Department of Molecular & Medical Pharmacology, University of California, Los Angeles, CA 90095-1595, USA

[d]School of Materials Science and Engineering, Tongji University, Shanghai 201804, China

† These authors contributed equally to this work.

To circumvent this problem, nanocomposites employing inorganic nanophosphors have been investigated as gamma sensitizers. $Ce_xLa_{1-x}F_3$ nanophosphors could be embedded in oleic acid to form gel-like transparent nanocomposites.[21] But such nanocomposites exhibit limited light yield and insufficient mechanical strength for practical uses. Epoxy nanocomposites embedded with BaF_2:Ce nanophosphors are also reported with limited success.[22] Nanocomposites comprising quantum dots dispersed in a conjugated polymer matrix have also been investigated; however, they were prepared by spin-coating and were only several hundred nanometers thick. They were too thin to attenuate high energy photons, since the mean free path of an X- or γ-ray in solid matter ranges from tens of microns to tens of centimeters depending on their energy.[23] Indeed, it has been a big challenge so far to achieve the desired transparency in the pursuit of gamma scintillating nanocomposites with the sufficient loading of nanocrystals, especially for the bulk size.

Here we demonstrate the synthesis of a new gamma scintillating composite based on polyvinyltoluene (PVT) as matrix. PVT has been the most widely used scintillating polymer for over 50 years due to its high scintillating efficiency, low cost and ease of fabrication. Gadolinium oxide (Gd_2O_3) nanocrystals are selected as the new gamma sensitizer, thanks to their wide band gap (5.2 eV) and modestly high atomic number. In this approach, the nanocrystals have a wider band gap than the CP matrix to suppress luminescence quenching. Transparent nanocomposites have been synthesized by thermally initiated bulk polymerization, containing up to 40% by weight of Gd_2O_3 nanocrystals dispersed in the polyvinyltoluene (PVT) matrix. Although Gd_2O_3 is not fluorescent, a high radioluminescence light yield can still be obtained in the polymer matrix by fulfillment of FRET and alleviation of Rayleigh scattering. The bulk nanocomposite scintillators are able to produce an appreciable resolved photoelectric peak upon gamma irradiation of 662 keV.

Results and discussion

Gadolinium oxide nanocrystals

Gd_2O_3 nanocrystals were synthesized *via* a modified thermal decomposition procedure.[24] The resulting nanocrystals were capped with oleic acid (OA) and oleylamine (OM), which are soluble in common organic solvents, such as toluene and hexanes. Transmission electron micrographs (TEM) of samples prepared from different solutions reveal a square nanoplate structure, rather than cubes. All nanocrystals deposited from a toluene solution lay on their faces on the TEM grid (Fig. 1A). When deposited from a hexanes solution, they tend to "stand" up on the grid (Fig. 1B). The measured edge length of the nanoplates is around 9 nm, and the thickness is about 1 nm, similar to observations reported in the literature.[25]

The structure and crystallinity of Gd_2O_3 nanocrystals were examined by X-ray Diffraction (XRD). As shown in Fig. 2A, XRD peaks are broadened due to the small size of nanocrystals compared to those of bulk Gd_2O_3. The two main peaks (2θ = 29.43 and 31.68) of monoclinic Gd_2O_3 (JCPDS file 43-1015) overlap, corresponding to the (4 0 1) and (3 1 0) crystallographic

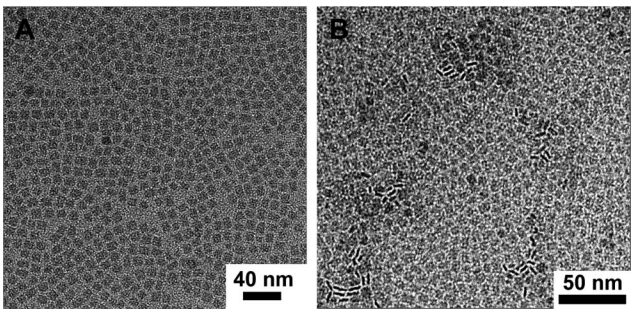

Fig. 1 TEM images of Gd_2O_3 nanocrystals capped with a mixture of OA and OM dispersed in toluene (A), and in hexanes (B).

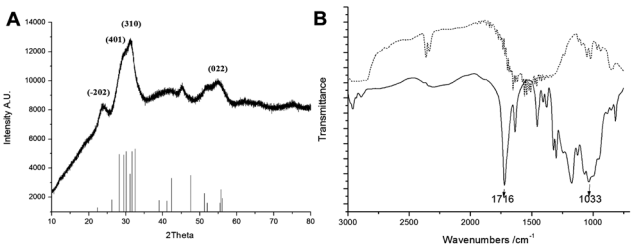

Fig. 2 XRD pattern (A) of Gd_2O_3 nanocrystals and FTIR spectra (B) of OA and OM-capped Gd_2O_3 nanocrystals (dashed line), and the BMEP-capped ones (solid line).

planes, respectively. This overlap makes it difficult to estimate the size of nanocrystals by using the Debye–Scherrer formula. The other peaks overlap with those from cubic Gd_2O_3 (JCPDS file 43-1014), making it difficult to determine if a single or double phase is present. The phase transition from cubic to monoclinic phase in Gd_2O_3 is size-dependent, and particularly occurs in the size range of 2–3 nm.[26,27] Thus, unambiguous phase identification is not trivial for the nanocrystals in this work. Further characterization by XRD is not carried out as the phase information should not affect the synthesis of the nanocomposites nor the intended application.

The OA/OM capped Gd_2O_3 nanocrystals were further modified by ligand exchange with bis(2-(methacryloyloxy)-ethyl) phosphate (BMEP), which was reported as the coupling agent to copolymerize metal oxide nanocrystals and methyl methacrylate.[28] The ligand exchange was monitored by Fourier transform infrared spectroscopy (FT-IR, Fig. 2B). The FT-IR spectrum of the BMEP-capped Gd_2O_3 nanocrystals shows peaks at 1716 and 1170 cm^{-1} that correspond to the vibration modes of C=O and C–C–O, respectively. The peaks at 1250 and 1033 cm^{-1} are assigned to the stretching vibration of P=O and P–O–CH_2, respectively.[29] In the spectrum of OA/OM capped Gd_2O_3 nanocrystals, the carbonyl peak is negligible, and the peak for P–O–CH_2 vibration does not exist. These differences in characteristic peaks confirm the ligand exchange with BMEP.

The ligand exchange was found to not affect the solubility, morphology, or crystallinity of the Gd_2O_3 nanocrystals. The XRD and TEM patterns of the BMEP-capped nanocrystals are identical to those of the OA/OM capped nanocrystals. Thermogravimetric analysis (TGA) of the nanocrystals showed that those

capped with OA/OM had 48% weight loss, whereas those capped with BMEP showed a weight loss of only 34% (Fig. 3A). Since BMEP, OA, and OM have similar molecular weights, and any phosphorus oxide residue formed would not contribute significantly to the ash weight, the large difference in TGA weight loss could likely be caused by different packing densities of the ligand on the metal oxide surface.[30,31] Despite the reduced number of ligands wrapping each nanocrystal, the BMEP-capped Gd_2O_3 nanocrystals also show good dispensability in toluene. The resulting transparent dispersion clearly indicates that the nanocrystals are uniformly distributed in the solvent, without appreciable agglomeration.

Gd_2O_3–PVT nanocomposites

Transparent nanocomposite monoliths were fabricated *via* thermally initiated free-radical bulk polymerization. Gd_2O_3 nanocrystals, as well as other additives, were dispersed in vinyltoluene to form a clear solution. In the selection of a suitable initiator, we note that aromatic initiators such as benzoyl peroxide could induce unexpected impurities and diminish the light yield of plastic scintillators.[32] An aliphatic peroxide, 1,1-di-(*tert*-butyl-peroxy)-3,3,5-tri-methylcyclohexane thus served as the thermal initiator. Its half lifetime at 95 °C is around 10 hours, which is suitable for polymerization of vinyltoluene. During the polymerization process, the initially clear solution in the vial remained transparent as it became viscous in half an hour and a rigid solid after being fully cured in 48 hours. The as-obtained monoliths were shaped as the interior of the vial. They were removed from the vial, polished to attain glossy surfaces, and used directly for various characterizations.

The loading content of Gd_2O_3 nanocrystals in the nanocomposites is expected to be the same as in the feed ratio of the polymerization solutions due to the nature of bulk polymerization. TGA was used to determine the actual content of the nanocrystals. The sample originally containing 40 wt% of nanocrystals showed a weight loss of 74% upon heating to 800 °C in air (Fig. 3A), with a 26% residue of Gd_2O_3 nanocrystals. The difference in the feed ratio is caused by the BMEP capping group which was also burnt off during the TGA analysis. It is in accordance with the measured loading content: the weight loss of BMEP-capped Gd_2O_3 nanocrystals in TGA is 34%; thus the 40 wt% loading of BMEP-capped nanocrystals corresponds to 40% × (1–34%), or 26.4%, of net nanocrystals in the nanocomposite. The density of Gd_2O_3 is 7.41 g cm^{-3}, and that of PVT is 1.05 g cm^{-3}. The calculated volume density of the Gd_2O_3 in the nanocomposite is calculated to be 4.6%. For convenience, the feed ratio, *i.e.*, 40 wt%, will be used to indicate the loading content.

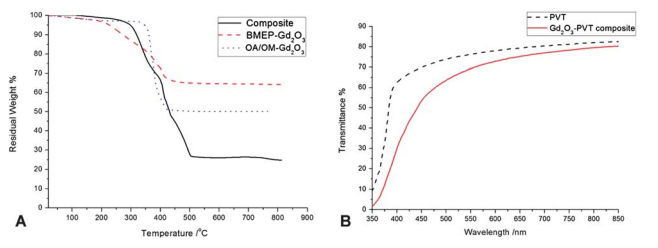

Fig. 3 (A) TGA curves of the OA/OM capped Gd_2O_3 nanocrystals (dotted curve), BMEP capped nanocrystals (dashed curve), and the nanocomposite containing 40 wt% loading of BMEP-capped nanocrystals (solid curve); (B) transmittance spectra of PVT (dashed curve) and the same nanocomposite (solid curve).

The nanocomposite monoliths exhibited good optical transparency along the visible region (Fig. 3B). The measured transmittance of the 3 mm thick sample containing 40 wt% of Gd_2O_3 nanocrystals is 69.6% at 550 nm (the wavelength of the scintillation emission peak). In most optical applications so far, interests have mainly focused on nanocomposites either with small thickness (normally below 1 micrometer) or in a dilute solution of nanocrystals[33–35] (normally below 10 wt%). It is thus of interest to investigate the transmittance of this nanocomposite system, where thickness and nanocrystal loading are both required.

The transmittance loss in the composite monolith is mainly caused by three factors: (1) the absorption of PVT and impurities, (2) the reflection on the two surfaces of the monolith, and (3) the Rayleigh scattering effect. The major transmittance loss in the UV range (below 400 nm) is due to the absorption of PVT, which has a long tail along the visible range. The reflection of light at the air–monolith interface is determined by the refractive index of the monolith, and is usually less than 10%.[36] Compared to the transmittance of the pure PVT monolith with the same thickness (76.0% at 550 nm), the nanocomposite has only a small portion of transmittance loss attributed to the Rayleigh scattering that resulted from the incorporation of nanocrystals, as is further discussed below.

The transmittance loss of the monolith as a result of Rayleigh scattering can be expressed as[37,38]

$$T = \frac{I}{I_0} = \exp\left[-\frac{32\pi^4 V_p x d^3 n_m^4}{\lambda^4}\left(\frac{\left(\frac{n_p}{n_m}\right)^2 - 1}{\left(\frac{n_p}{n_m}\right)^2 + 2}\right)^2\right] \quad (1)$$

where x is the optical path length or distance between the parallel surfaces of the monolith, V_p and d are, respectively, the volume fraction and diameter of embedded nanoparticles, λ is the wavelength of light, n_p and n_m are, respectively, the refractive indices of the nanoparticles and the matrix. If the ratio of the refractive indices $n_p : n_m$ is kept close to 1, high optical transparency across a thick nanocomposite with high nanoparticle loading is achieved.[22] In the Gd_2O_3–PVT nanocomposites, $n_p : n_m = 1.80 : 1.55$. And the fairly small n_p of Gd_2O_3 among heavy metal oxides leads to this high transmittance. When $x = 3$ mm, $d \sim 9$ nm at 550 nm, the Rayleigh scattering governed transmittance is calculated to be 96.0% for nanocomposites with 40 wt% loading of nanocrystals (V_p = 4.6%). As a reference, if n_p is increased to 2.4 (the value of TiO_2) and other conditions are kept the same, the transmittance drops to 78.6%.

According to the equation, the transmittance is governed by nanoparticle size as well: the aggregation of nanoparticles would increase the Rayleigh scattering effect. In the Gd_2O_3–PVT nanocomposite with 31 wt% loading, severe aggregation of

nanocrystals is barely observed in its TEM image as shown in Fig. 4. The contrast of the nanocrystals against the PVT matrix is rather low, possibly because of the small thickness of the nanocrystals. Some dark spots in the image are observed with a feature size of about 10 nm, which possibly resulted from the aggregation of the nanocrystals. However, it could also be caused by the overlaps of the nanoparticles in the projection of electron beams, which does not necessarily indicate aggregations. In general, the dispersion is considered fairly uniform, and BMEP capping molecules play a key role in it. The phosphoric acid group on one end of BMEP can form a stronger bond with the metal oxide surface than the carboxylic acid group in OA and the amino group in OM, and therefore is expected to obtain a relatively stable surface coverage.[39] The dangling methacrylate groups on the other end of the BMEP molecule can copolymerize with VT, and thus covalently bond the BMEP molecules onto the PVT matrix. Ligands containing polymerizable groups have been demonstrated to alleviate the aggregation of nanocrystals in polymer composites.[40] BMEP helps anchor the Gd_2O_3 nanocrystals to the PVT matrix, and results in their distribution. Therefore, the resulting bulk nanocomposites could be transparent.

Photoluminescence and scintillation

Gd_2O_3 is a wide bandgap material. As shown in Fig. 5A, the absorption spectrum of the nanocrystal shows a peak at 240 nm corresponding to a band gap of 5.2 eV. The nanocrystals have a very weak emission (not shown in the figure) with a maximum at 410 nm, which is due to the surface defects commonly observed in non-fluorescent metal oxide nanocrystals. The absorption and emission spectra of the PVT film are presented in Fig. 5A. The absorption maximum at ~310 nm and the emission maximum at ~330 nm are in accordance with the reported PVT excimer characteristics.[41,42] Fig. 5A also exhibits the photoluminescence spectrum of the fluor, namely, 4,7-bis-{2′-9′,9′-bis[(2′′-ethylhexyl)-fluorenyl]}-2,1,3-benzothiadiazole (FBtF), dissolved in hexanes. It showed an emission peak at 520 nm and two excitation maxima, at 310 nm and 420 nm, respectively.

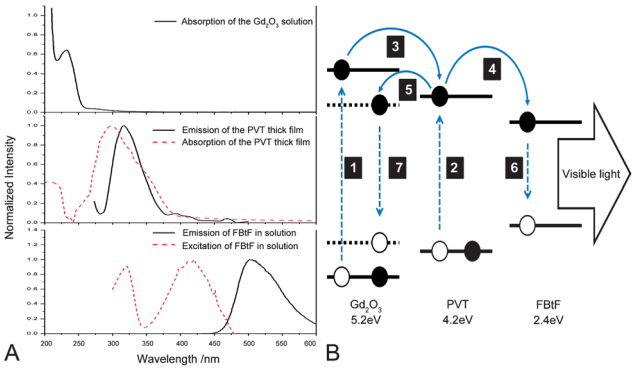

Fig. 5 Optical spectra (A) of different components and schematic illustration (B) of scintillation photophysics in the composites. (A) shows the UV absorption spectrum of Gd_2O_3 nanocrystals in hexanes (upper), the absorption (middle, dashed curve) and emission (middle, solid curve) spectra of the PVT thick film, and the excitation (bottom, dashed curve) and emission spectra (bottom, solid curve) of FBtF in hexanes.

It is argued that FRET takes place from PVT to the fluor, and the incorporation of Gd_2O_3 nanocrystals does not affect this process. As illustrated in Fig. 5B, upon irradiation on the nanocomposite, excitons are generated on Gd_2O_3 nanocrystals and the PVT matrix, respectively (processes 1 and 2). Most excitons on the nanocrystals are inclined to transfer energy to the surrounding polymer matrix (process 3) driven by an energy level difference. In contrast, those on the PVT matrix do not back-transfer to nanocrystals, but transfer to the fluors and decay radiatively (processes 4 and 6). FRET takes place efficiently,[43] because the excitation peak of the fluor overlaps well with the characteristic emission peaks of PVT, and the distance between the fluor and PVT reaches the critical radius at this concentration. Additional evidence is obtained in the scintillation measurement, as will be discussed in the following paragraphs. However, a tail was observed in the absorption spectra of the nanocrystals starting at 300 nm, likely due to surface states on the nanocrystals. These surface states may serve as sinks to trap some excitations either on nanocrystals or polymers (processes 5 and 7), but can be eliminated by surface engineering.

Beta-induced radioluminescence spectra were acquired from nanocomposites containing 31 wt% and 40 wt% Gd_2O_3 nanocrystals (Ø 14 mm × 3 mm), and are shown in Fig. 6A. Both samples have emission maxima at 530 nm, consistent with the emission spectrum of FBtF, the fluor used in both nanocomposites. The light yield of the nanocomposite scintillators was obtained by comparing the emission flux of the composite at steady state upon irradiation of ^{204}Tl to that of BC400, which is a commonly used plastic scintillator with a light yield of ~13 000/MeV. The beta light yields of the nanocomposites containing 31 wt% and 40 wt% of nanocrystals are found to be

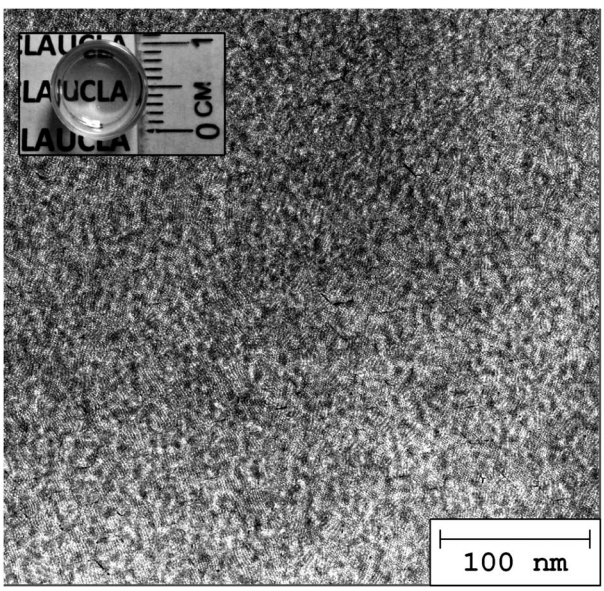

Fig. 4 TEM image of a nanocomposite (31 wt% loading of nanocrystals) slice with 90 nm thickness prepared by ultramicrotomy. The inset is the optical photograph of the 3 mm thick nanocomposite disk.

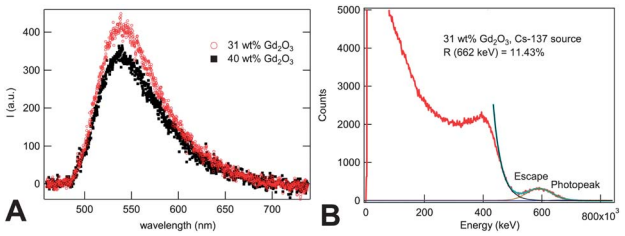

Fig. 6 Beta radioluminescence spectra (A) acquired from samples with 31 wt% (open circle) and 40 wt% (solid square) loading of Gd_2O_3 nanocrystals (Ø 14 mm × 3 mm) and gamma pulse height spectrum (B) acquired from the sample with 31 wt% loading upon irradiation with ^{137}Cs.

210% and 170%, respectively, relative to BC400. The light yields of the nanocomposites are therefore calculated to be 27 000/MeV and 22 000/MeV.

The decay time constant of the composite scintillators was measured by placing the samples on the photocathode of a (PMT Hamamatsu R2083) upon irradiation of ^{204}Tl. The decay time is 17 ns, in the same time scale as for the fluor's fluorescence decay. It is generally accepted that the introduction of quenchers in scintillators not only diminishes light output, but also decreases scintillation decay time.[44] The high light yield and the observed decay time being the same as the fluor indicate that Gd_2O_3 nanocrystals in the nanocomposite do not considerably interfere with the FRET between PVT and the fluors.

With increased Z and density, Gd_2O_3 nanocrystals are expected to improve the gamma sensitivity in the composite scintillators. The pulse height spectrum of the 31 wt% Gd_2O_3 loaded nanocomposite scintillator is obtained by using a ^{137}Cs irradiation source, as shown in Fig. 6B. It exhibits a photopeak at 662 keV and the Compton edge at 400 keV. A Gaussian fit revealed energy resolution at 662 keV of 11.4%. The increased Z_{eff} leads to the appearance of the photopeak in the nanocomposite, because the photoelectric ratio is proportional to Z_{eff}^{n} (n varies from 3 to 5). The Z_{eff} of the nanocomposite is calculated following the equation[45]

$$Z_{eff} = \sqrt[3]{f_1 Z_1^{\,3} + f_2 Z_2^{\,3} + \ldots} \quad (2)$$

where f_n is the fraction of the total number of electrons of element n in the composite, and Z_n is the atomic number of element n. The value is calculated to be 28.0 for the nanocomposite with 4.6 vt% loading of nanocrystals. As a reference, plastic scintillators without the addition of high-Z components have a Z_{eff} of ~5.8. The density of the nanocomposite is 1.2 g cm^{-3}, which is also higher than that of plastic scintillators (~1.05 g cm^{-3}). High density increases the scintillator's stopping power for gamma rays, and reduces the escape peak intensity.

It is further noted that the PMT used (Hamamatsu R6231-100) has a quantum efficiency of merely ~8% at 550 nm, which is the emission maximum of the composite scintillator. The scintillation detection process obeys the Poisson distribution, and the energy resolution in the pulse height spectrum is limited statistically by the equation[3]

$$R|_{limit} = 2.35\sqrt{\frac{1}{N}} \quad (3)$$

where N is the number of photons collected by the PMT to generate signals. It is thus reasonable to argue that the same nanocomposite would have produced a photopeak with better energy resolution when a PMT with higher quantum efficiency at 550 nm was applied. Theoretically, by using a PMT with a quantum efficiency of 24% at 550 nm, the same system would produce an energy resolution limit of 6.1%.

Conclusions

A nanocomposite comprised of Gd_2O_3 nanocrystals embedded in the PVT matrix has been fabricated for gamma-ray spectroscopy. Highly transparent, cubic centimeter-size composite samples were obtained by bulk polymerization of the nanocrystal solution in the monomer. Incident gamma rays interact with the nanocrystals *via* photoelectric effects to produce photoelectrons, which further excite the polymer matrix leading to the production of visible photons from the fluor. The as-prepared nanocomposite scintillator shows a beta light yield of 27 000/MeV, more than twice that of conventional plastic scintillators. Gamma radiation at 622 keV produces a photopeak with 11.4% energy resolution.

The work has resolved two important issues in the synthesis of composite scintillators: transparency and light yield. To minimize luminescence quenching commonly encountered in composite synthesis, a wide band gap gamma photosensitizer is employed in this approach. The conjugated polymer matrix has a wider band gap than sensitizers. Excitons generated during the attenuation of the high velocity photoelectron are predominantly transferred to the fluor *via* the FRET mechanism. The high transparency of the bulk-size nanocomposite with relatively high loading of nanocrystals has been obtained as a result of (1) the small difference of refractive indices of the nanocrystals and the polymer matrix; (2) small size and uniform distribution of the nanocrystals; and (3) the employment of a multifunctional ligand molecule that helps anchor the nanocrystals to the polymer chains *via* copolymerization.

Experimental

Materials

Gadolinium(III) acetate hydrate (99.9%), oleic acid (OA, 99%), oleylamine (OM, 80%), methylstyrene, bis(2-(methacryloyloxy)-ethyl) phosphate (BMEP), and 1,1-di-(*tert*-butyl-peroxy)-3,3,5-trimethylcyclohexane (75% solution in aromatic free mineral spirit, DTTMC) were purchased from Sigma-Aldrich and used as received.

Synthesis

The Gd_2O_3 nanocrystal synthesis followed synthetic procedures reported in ref. 24 with modifications. Typically, gadolinium(III) acetate hydrate (3.35 g) was added into OA (8.7 g) and OM (5.8 g) at room temperature. The slurry was heated to 135 °C and kept

for 2 h with vigorous magnetic stirring under vacuum to remove water and oxygen. The thus-obtained optically transparent solution was heated to 330 °C and kept for 1.5 h. The white products were obtained by adding acetone (90 ml) to the reacted solution, washed by ethanol (90 ml), and centrifugation and vacuumed with a yield of 2.0 g in total.

For ligand exchange, 0.8 g of Gd_2O_3 nanoparticles capped with oleic acid and oleylamine was dispersed in 0.64 g BMEP dissolved in 30 ml chloroform. The mixture was stirred overnight. Chloroform was then removed by rotary evaporation to obtain a viscous solid, which was washed with ethanol. The as-obtained white suspension was centrifuged, and the white product was dried in vacuum for 2 h.

To synthesize nanocomposites, BMEP capped Gd_2O_3 nanocrystals (0.34 g), 4,7-bis-{2′-9′,9′-bis[(2″-ethylhexyl)-fluorenyl]}-2,1,3-benzothiadiazole (FBtF, 13 mg), methylstyrene (VT, 0.59 g), and DTTMC (0.1 wt%) were placed in a vial and shaken to form a transparent solution. The polymerization was conducted at elevated temperatures. The as-obtained nanocomposite monoliths were machined to obtain a mirror finish.

Characterizations

XRD was carried out with a Panalytical X'Pert Pro Powder Diffractometer using CuKα radiation. TEM was conducted on a FEI CM120 microscope operated at 120 kV. The nanocomposite slices of 90 nm were prepared by a UTC ultramicrotome. The FTIR spectrum was obtained using a JASCO FT/IR-420 spectrometer. Samples were prepared by drop-casting a nanocrystal dispersion (in toluene) onto a KBr crystal and allowing the solvent to evaporate to form a thin solid coating of the nanocrystals. TGA was performed on a Perkin-Elmer Thermal Analysis Pyris Diamond TG/DTA instrument, samples were heated from room temperature to 800 °C at a rate of 10 °C min^{-1} in air. Fluorescence spectra were measured with a PTI QuantaMaster 30 spectrofluorometer. Transmittance of monoliths was acquired by using a Shimadzu UV-1700 spectrophotometer. The light yield was measured in an IVIS Lumina II system (Caliper Life Sciences) with an irradiation source of ^{204}Tl. The decay time of the scintillator was measured by an R2083 PMT coupled with a Tektronix TDS 3064B oscilloscope under the irradiation of ^{204}Tl. All measured samples were wrapped with PTFE at the peripheral with one face directly coupled to the irradiation source. The radioluminescence spectra were acquired using a $^{90}Sr/^{90}Y$ source, and were collected with a Princeton Instruments/Acton Spec 10 spectrograph coupled to a thermoelectrically cooled CCD camera and corrected for spectral sensitivity. The pulse-height spectra were acquired using the 662 keV gamma rays from ^{137}Cs. A Hamamatsu R6231-100 superbialkali PMT was used to collect signals, which were shaped with a Tennelec TC 244 spectroscopy amplifier and recorded with an Amptek MCA8000-A multi-channel analyzer. The pulse-height spectra were fit to two Gaussians, representing the photopeak and the escape peak (due to the escape of the Bi X-rays at 76 and 83 keV). The escape peak is the dominant feature, due to the small sample sizes, but should be eliminated for large (>5 in^3) scintillators.

Acknowledgements

This work was supported by the Defense Threat Reduction Agency of the United States Department of Defense, Contract # HDTRA1-07-1-0028. W.C. acknowledges the financial support of the China Scholarship Council. The LLNL contribution is funded by the U.S. DOE, NNSA, Office of Defense Nuclear Nonproliferation, Office of Nonproliferation Research and Development (NA-22).

Notes and references

1 P. Gomez-Romero, *Adv. Mater.*, 2001, **13**, 163.
2 F. Hussain, M. Hojjati, M. Okamoto and R. E. Gorga, *J. Compos. Mater.*, 2006, **40**, 1511.
3 G. F. Knoll, *Radiation Detection and Measurement*, Wiley, Hoboken, N.J., 4th edn, 2010.
4 B. D. Milbrath, A. J. Peurrung, M. Bliss and W. J. Weber, *J. Mater. Res.*, 2008, **23**, 2561.
5 L. J. Basile, *J. Chem. Phys.*, 1957, **27**, 801.
6 M. Hyman, Jr and J. J. Ryan, *IRE Trans. Nucl. Sci.*, 1958, **5**, 87.
7 S. R. Sandler and K. C. Tsou, *Int. J. Appl. Radiat. Isot.*, 1964, **15**, 419.
8 S. R. Sandler, J. Dannin and K. C. Tsou, *J. Polym. Sci., Part A: Gen. Pap.*, 1965, **3**, 3199.
9 Z. H. Cho, C. M. Tsai and L. A. Eriksson, *IEEE Trans. Nucl. Sci.*, 1975, **NS22**, 72.
10 Y. S. Zhao, Z. B. Yu, A. Douraghy, A. F. Chatziioannou, Y. Q. Mo and Q. B. Pei, *Chem. Commun.*, 2008, 6008.
11 G. I. Britvich, V. G. Vasil'chenko, V. G. Lapshin and A. S. Solov'ev, *Instrum. Exp. Tech.*, 2000, **43**, 36.
12 M. Hamel, G. Turk, A. Rousseau, S. Darbon, C. Reverdin and S. Normand, *Nucl. Instrum. Methods Phys. Res., Sect. A*, 2011, **660**, 57.
13 J. L. Kropp and M. Burton, *J. Chem. Phys.*, 1962, **37**, 1752.
14 S. R. Sandler and K. C. Tsou, *J. Phys. Chem.*, 1964, **68**, 300.
15 A. Hallam and J. B. Birks, *J. Phys. B: At. Mol. Phys.*, 1978, **11**, 3273.
16 H. Z. Zhong, Y. S. Zhao, Y. F. Li and Q. B. Pei, *Nanotechnology*, 2008, **19**, 505503.
17 Y. S. Zhao, H. Z. Zhong and Q. B. Pei, *Phys. Chem. Chem. Phys.*, 2008, **10**, 1848.
18 B. L. Rupert, N. J. Cherepy, B. W. Sturm, R. D. Sanner and S. A. Payne, *Europhys. Lett.*, 2012, **97**, 22002.
19 W. V. Steele, *J. Chem. Thermodyn.*, 1979, **11**, 187.
20 D. H. Hey, D. A. Shingleton and G. H. Williams, *J. Chem. Soc.*, 1963, 5612.
21 R. K. Feller, G. M. Purdy, D. Ortiz-Acosta, S. Stange, A. Li, E. A. McKigney, E. I. Esch, R. E. Muenchausen, R. Gilbertson, M. Bacrania, B. L. Bennett, K. C. Ott, L. Brown, C. S. Macomber, B. L. Scott and R. E. Del Sesto, *J. Mater. Chem.*, 2011, **21**, 5716.
22 Z. T. Kang, M. Barta, J. Nadler, B. Wagner, R. Rosson and B. Kahn, *J. Lumin.*, 2011, **131**, 2140.
23 I. H. Campbell and B. K. Crone, *Adv. Mater.*, 2006, **18**, 77.

24 R. Si, Y. W. Zhang, H. P. Zhou, L. D. Sun and C. H. Yan, *Chem. Mater.*, 2007, **19**, 18.
25 Y. C. Cao, *J. Am. Chem. Soc.*, 2004, **126**, 7456.
26 S. Seo, H. Yang and P. H. Holloway, *J. Colloid Interface Sci.*, 2009, **331**, 236.
27 Y. Wang, O. Milosevic, L. Gomez, M. E. Rabanal, J. M. Torralba, B. Yang and P. D. Townsend, *J. Phys.: Condens. Matter*, 2006, **18**, 9257.
28 Z. Shan, W. S. Yang, X. Zhang, Q. M. Huang and H. Ye, *J. Braz. Chem. Soc.*, 2007, **18**, 1329.
29 J. Jang and Y. K. Jeong, *Fibers Polym.*, 2008, **9**, 667.
30 S. Pawsey, K. Yach and L. Reven, *Langmuir*, 2002, **18**, 5205.
31 I. Langmuir, *Proc. Natl. Acad. Sci. U. S. A.*, 1917, **3**, 251.
32 P. V. Kulkarni, P. P. Antich, J. A. Anderson, J. Fernando, T. M. Aminabhavi, S. F. Harlapur, M. I. Aralaguppi and R. H. Balundgi, *Polym.-Plast. Technol. Eng.*, 1997, **36**, 1.
33 M. M. Demir, P. Castignolles, Ü. Akbey and G. Wegner, *Macromolecules*, 2007, **40**, 4190.
34 D. Sun, H. J. Sue and N. Miyatake, *J. Phys. Chem. C*, 2008, **112**, 16002.
35 B. Davion, V. Delhorbe, S. Peralta, F. Goubard and F. Vidal, *J. Nanosci. Nanotechnol.*, 2011, **11**, 3208.
36 W. D. Callister and D. G. Rethwisch, *Materials Science and Engineering: An Introduction*, John Wiley & Sons, Hoboken, NJ, 8th edn, 2010.
37 B. M. Novak, *Adv. Mater.*, 1993, **5**, 422.
38 C. L. Lu and B. Yang, *J. Mater. Chem.*, 2009, **19**, 2884.
39 P. Kim, S. C. Jones, P. J. Hotchkiss, J. N. Haddock, B. Kippelen, S. R. Marder and J. W. Perry, *Adv. Mater.*, 2007, **19**, 1001.
40 S. X. Zhou, G. Garnweitner, M. Niederberger and M. Antonietti, *Langmuir*, 2007, **23**, 9178.
41 Z. Polacki, *J. Polym. Sci., Polym. Phys. Ed.*, 1984, **22**, 2275.
42 B. G. Giren and Z. Polacki, *J. Photochem. Photobiol., A*, 1990, **52**, 321.
43 T. Forster, *Ann. Phys.*, 1948, **2**, 55.
44 J. B. Birks, *The Theory and Practice of Scintillation Counting*, Pergamon Press, distributed in the Western Hemisphere by Macmillan, Oxford, New York, 1964.
45 R. C. Murty, *Nature*, 1965, **207**, 398.

